Journal of the European Ceramic Society **15** (1995) 415–424

0955-2219/95/$9.50

0955-2219(95)00008-9

The Development of Microstructure in Silicon Nitride-Bonded Silicon Carbide

D. P. Edwards,[a,c] B. C. Muddle,[a] Y.-B. Cheng[a] & R. H. J. Hannink[b]

[a]Department of Materials Engineering, Monash University, Clayton, Victoria, 3168, Australia
[b]C.S.I.R.O. Division of Material Science and Technology, Private Bag 33, Rosebank MDC, Clayton, Victoria, 3169, Australia

(Received 6 May 1994; revised version received 14 October 1994; accepted 12 December 1994)

Abstract

The microstructure of a commercial silicon nitride-bonded silicon carbide ceramic composite, formed via the nitridation of silicon powder–SiC preforms, has been characterised using analytical transmission electron microscopy. It comprised coarse particles of SiC dispersed in a matrix which was a mixture of crystalline phases based on Si_2N_2O and β-Si_3N_4, and an amorphous phase. Qualitative microanalysis of amorphous matrix regions revealed the presence of significant concentrations of aluminium, silicon, calcium and oxygen, while aluminium and oxygen were also readily detectable in both of the surrounding crystalline phases. It is thus suggested that the crystalline phases in the matrix are in fact O- and β-sialons respectively. A mechanism, combining reaction bonding and solution-precipitation in a (Ca,K)–aluminosilicate liquid phase at the reaction temperature, is proposed to describe the development of the matrix microstructure.

1 Introduction

The potential for near net shape forming of Si_3N_4 ceramics via the direct nitridation of silicon compacts, together with the economic advantage inherent in the use of silicon powder compared with currently available Si_3N_4 powders, have been major factors in sustaining continued interest in the application of the reaction bonding process to these ceramics in recent years. However, the consolidated densities achieved using this approach are typically only 80% of those obtainable by hot pressing techniques and the lower density, combined with the continuous nature of the porosity typical of reaction-bonded compacts, continue to limit the applications of such materials.

One approach to overcoming these difficulties has involved the development of the nitrided pressureless sintering (NPS) technique,[1–4] which combines the nitridation process with a liquid phase sintering stage, promoted through the addition of oxide sintering aids to silicon/Si_3N_4 compacts. This technique has been shown to be capable of producing Si_3N_4-based materials with near to theoretical densities and, with improved composition control and tailoring of the final microstructure, has the potential to allow more economical production of materials exhibiting reduced shrinkage during sintering and minimal porosity.

The Si_3N_4-based materials developed in this way have potential for application as the bonding constituents in low cost composite refractory materials, typically containing a major fraction of silicon carbide aggregate.[5] Such binders offer potentially superior oxidation and alkali resistance in molten metal environments compared with alumino–silicate matrices in current usage.[6,7] There is thus ongoing interest in the characterisation of the microstructure of such materials and in elucidating the stages of microstructural evolution during the sintering cycle.

The purpose of the present paper is to report on the microstructural characterisation of a commercially produced, reaction-bonded Si_3N_4–SiC composite, containing significant oxide additions, predominantly in the form of a clay binder. This work forms part of a larger project currently being undertaken to examine, using analytical transmission electron microscopy, the microstructural development of Si_3N_4-based ceramics produced by the NPS technique.

2 Experimental Procedures

Fabrication of the composite involved the wet blending of the major components, Si powder (particle size <44 μm) and crushed SiC (70–650

[c]Present address: Defence Science and Technology Organisation, Aeronautical and Maritime Research Laboratories, P.O. Box 4331, Melbourne, Victoria, 3001, Australia.

μm, in the approximate weight ratio of 1:3, with minor additions of organic plasticising agent (Ca–lignosulphonate) and clay (≤5 wt%) to aid plasticity of the slurry prior to moulding of the composite preforms. The cast preforms were allowed upwards of 8 h for material sedimentation and water extraction before mould removal. Sintering of the preforms was carried out in an N_2 atmosphere using a slow heating cycle, with a binder–burnout stage at 400–600°C, a final sintering temperature of 1450°C and a sintering time in excess of 20 h.

Initial phase analysis of the composite was performed in a Siemens D500 powder X-ray diffractometer using Ni-filtered Cu K_α radiation. Lattice parameters of the phases were determined from the measured X-ray diffraction peaks using a least squares fitting routine within the Celsiz program,[8] with calibration performed using silicon as an internal standard.

Composite surfaces for optical and scanning electron microscopy (SEM) were prepared by initial polishing of bulk specimens on a tin lap, followed by final 1 μm diamond polishing. Polished samples were examined in a JEOL 840A scanning electron microscope operating at 20 kV. Specimens for transmission electron microscopy (TEM) were prepared by diamond cutting thin composite slices, grinding and polishing to form 120 μm thick discs, and finally ion milling these discs to electron transparency using 5 kV argon ion beams at an incident angle of 15°. The specimens were coated with a thin carbon film and examined in a Philips CM20 analytical electron microscope operated at 200 kV and equipped with an ultra-thin window Link energy dispersive X-ray spectrometer (EDXS). For comparative X-ray microanalysis, an electron probe of nominally 10 nm diameter was used routinely in the scanning transmission electron microscope (STEM) mode.

3 Experimental Results

3.1 X-ray diffraction

The X-ray diffractometer trace from the reaction-bonded composite, Fig. 1, indicates that, in addition to SiC, the major crystalline phases in the composite are silicon oxynitride (Si_2N_2O) and β-Si_3N_4, with minor fractions of α-Si_3N_4 and unreacted silicon also present. The relative fractions of Si_2N_2O and β-Si_3N_4 in the binder phase were calculated as approximately 0·6 and 0·4 respectively, employing a technique making use of the (002) Si_2N_2O and (210) β-Si_3N_4 peak intensities[9] and ignoring minor phases. Efforts to determine more accurately the phase content of the matrix and the polytypes of SiC present, using available crystallographic data and a Rietveld analysis,[10] proved difficult due to the presence of multiple phases and significant overlap of diffraction peaks. However, analysis of the SiC peaks from both the composite and the starting SiC powder indicated that the 6H structure was the dominant polymorph, with the presence of the cubic (3C) and other α-polytypes as minor constituents suggested by the asymmetry of several major peaks.

A systematic shift in the peak positions for the Si_2N_2O and β-Si_3N_4 phases to lower diffraction

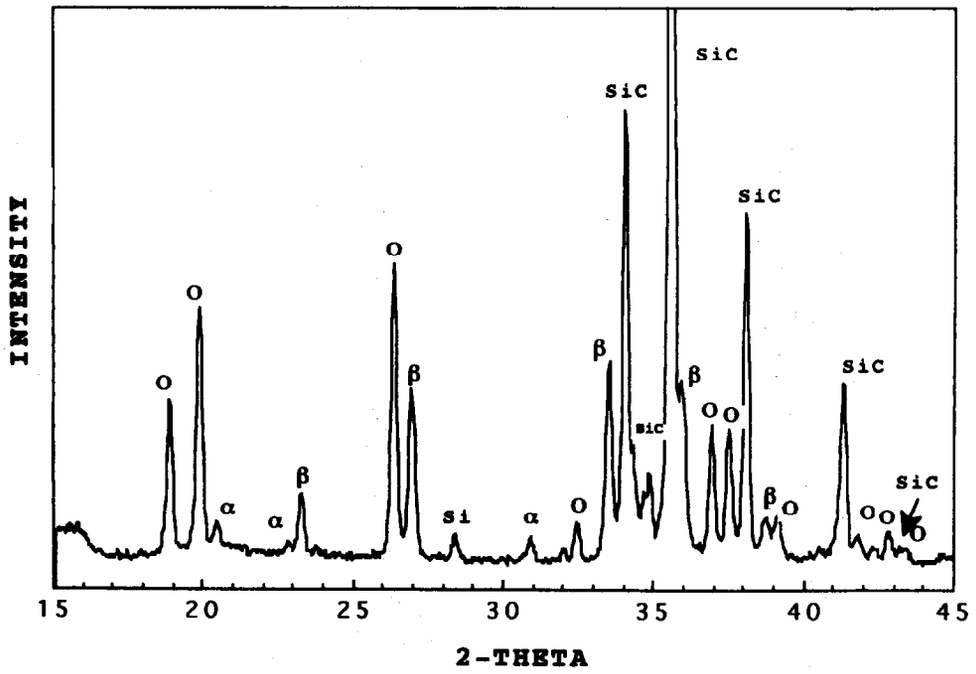

Fig. 1. X-ray diffractometer trace from as-fired material indicating the presence of SiC in a matrix that is predominantly a mixture of crystalline phases based on β-Si_3N_4 and Si_2N_2O (O).

angles (2θ) was noted, when compared with expected positions for the pure compounds. The lattice parameters of the hexagonal β-Si_3N_4 were determined to be a = 0·7617 ± 0·0004 nm and c = 0·2923 ± 0·0003 nm, while those of the orthorhombic oxynitride were measured to be a = 0·8909 ± 0·0003 nm, b = 0·5505 ± 0·0001 nm and c = 0·4861 ± 0·0001 nm. These values are systematically larger than those normally quoted for the pure compounds,[11] and are consistent with an expansion in the unit cell that might arise through Al–O bond substitution for Si–N bonds during sintering.

It is unlikely that the Si_2N_2O within the matrix can be attributed solely to the SiO_2 that is expected to be introduced as a surface layer on both the silicon and SiC powders. The high content of crystalline Si_2N_2O observed, and the almost exclusive appearance of β-Si_3N_4 in preference to α-Si_3N_4, suggest the presence of a liquid phase during the 1450°C reaction bonding process if proposed solution–reprecipitation mechanisms for Si_2N_2O formation are correct.[12–14] This is consistent with the presence in the original powder mixture of additional glass-forming oxides, which will promote the formation of a low melting point liquid and provide a source of oxygen for the formation of Si_2N_2O. However, the lack of a broad low-angle diffraction peak characteristic of an amorphous phase in the X-ray diffractometer trace of Fig. 1 implies that there is a low level of residual glass remaining within the composite after firing.

A few minor peaks remain unidentified in the X-ray diffractometer trace and are suspected to arise from metallic impurities introduced into the raw materials during powder processing.

3.2 Optical and scanning electron microscopy

Figure 2 is an optical micrograph typical of an unetched, polished surface of the as-fired composite, where the large silicon carbide grains in light grey contrast range in size from 20 to 450 μm and constitute approximately 75 vol.% of the composite microstructure. The microstructure of the Si_2N_2O–Si_3N_4 binder is unresolved at this scale, but it appears that it forms a near continuous, cohesive bond around the entire perimeter of the silicon carbide particles. The local dark areas within the binder represent a combination of intrinsic pores and defects introduced during polishing.

Examination in the scanning electron microscope, using backscattered electron contrast, revealed the presence of an impurity phase in light contrast at the SiC boundaries, Fig. 3, while the larger SiC grains often contained a core of slightly darker contrast. Energy dispersive X-ray spectroscopy of the two phases in light contrast (arrowed A and B respectively) indicated significant concentrations of Si, Fe and other metallic impurities, Fig. 3(b), in regions A, while in regions B, unreacted Si alone was detected. Optical and scanning electron microscopy of the raw SiC powder established the presence of the same phases intimately associated with the original SiC particles and it is thus inferred that these phases arise during the processing of the SiC. The use in the composite system of SiC produced by the reaction sintering method is the most likely source of additional metallic impurities in the microstructure, as

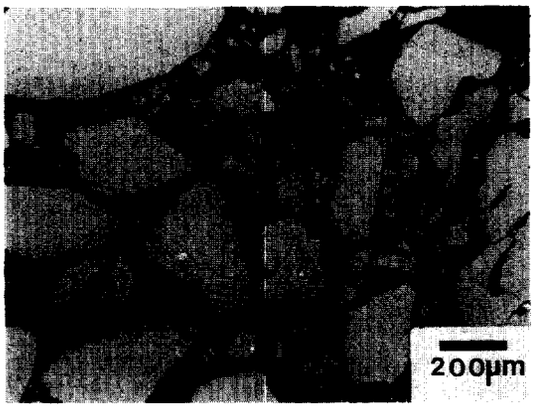

Fig. 2. Reflected light micrograph of unetched, polished surface of as-fired composite.

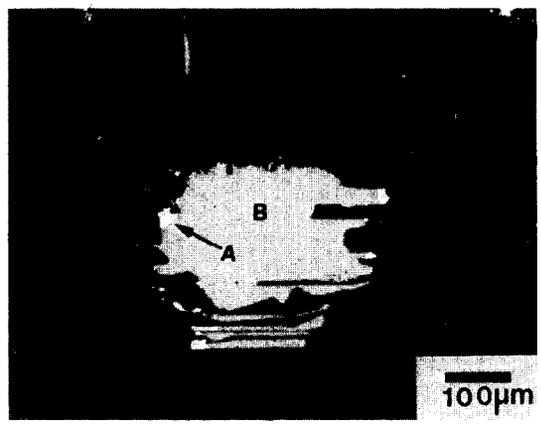

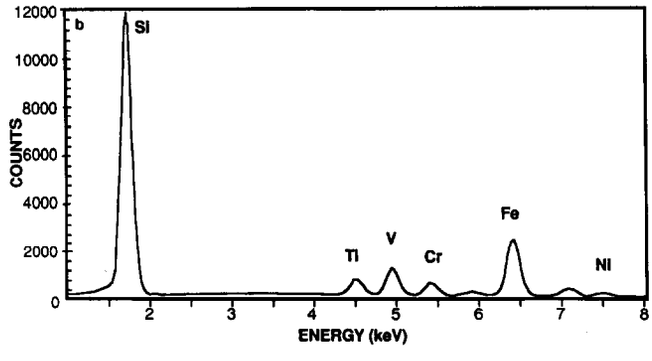

Fig. 3. (a) Backscattered electron image of as-fired composite showing impurity phase (regions A) and unreacted silicon (region B) within SiC grain, and (b) energy dispersive X-ray spectrum typical of impurity phase A.

reaction-sintered SiC is known to contain up to 10% unreacted silicon and other silicide impurities in the final product.[15]

3.3 Transmission electron microscopy

The microstructure of the binder in the composite was complex and varied significantly in grain size and morphology between thin foil specimens and even between adjacent areas within the same sample. Such variability is perhaps related to the relatively large scale of the initial SiC particles, resulting in poor mixing of the raw materials and/or segregation of components during green fabrication, which prevent the formation of a homogeneous structure. Figure 4(a) is a bright field TEM image showing a representative area of the binder microstructure, in which each of the grains in this field has been identified by electron microdiffraction to be either crystalline β-Si_3N_4 (β) or Si_2N_2O (O), while the central region is residual amorphous phase (G). Figures 4(b) and (c) show representative electron microdiffraction patterns used to identify the silicon nitride grains, indexed as (b) [0001] and (c) [$10\bar{1}0$] zone axis patterns from the hexagonal β-Si_3N_4 structure. The Si_3N_4 formed in a variety of morphologies, ranging from approximately equiaxed grains with smoothly curved surfaces and an average diameter of 350 nm, Fig. 4(a), to grains with a faceted, rod-like form. Those elongated grains, which were relatively rare, had a morphology commonly considered typical of the product of the α–β phase transformation in systems containing a liquid phase.[16–18]

In contrast to the Si_3N_4, the Si_2N_2O grains (50–500 nm) were readily distinguished by their elongated, faceted morphology[19,20] and a substructure of stacking faults parallel to the long axis, Fig. 5(a). The Si_2N_2O was also noted to have a tendency to form grains with faceted ends, with the angle of contact between grains apparently being determined by such facet angles. The form of the relationship between such contiguous crystals is at present the subject of further study. Figures 5(b) and (c) show representative electron microdiffraction patterns recorded from the Si_2N_2O grains, which may be indexed as (b) [$1\bar{1}0$] and (c) [$\bar{1}01$] zone axis patterns from the orthorhombic oxynitride structure.[21]

Non-crystalline regions observed within the binder microstructure were also identified by diffraction and diffraction contrast techniques.[22] As shown in Fig. 6, the glass had formed as discrete pockets at three and four grain junctions involving both oxynitride and β-Si_3N_4 grains, and was not readily detectable in the form of continuous intergranular films. The incidence of amorphous

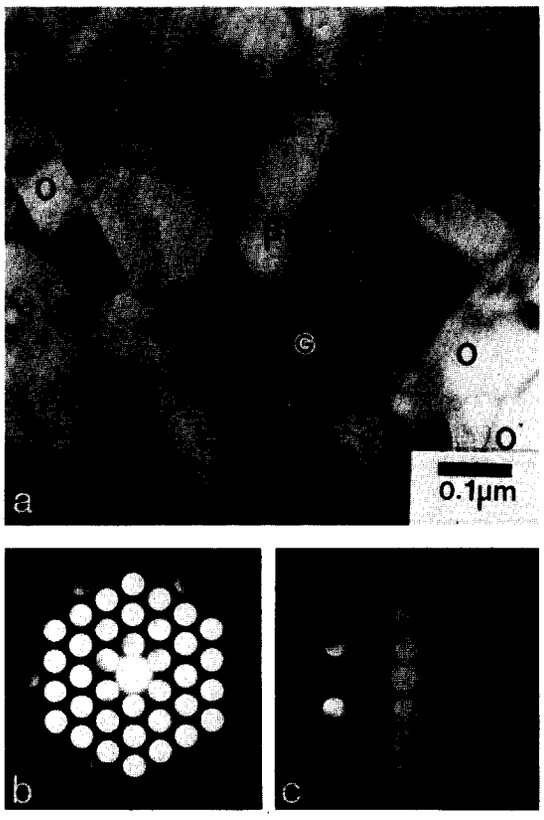

Fig. 4. (a) Transmission electron micrograph showing region of amorphous phase (G) surrounded by a mixture of crystalline phases based on β-Si_3N_4 and Si_2N_2O (O), and electron microdiffraction patterns which can be indexed unambiguously as (b) [0001], and (c) [$10\bar{1}0$] zone axis patterns from the hexagonal β-Si_3N_4 structure.

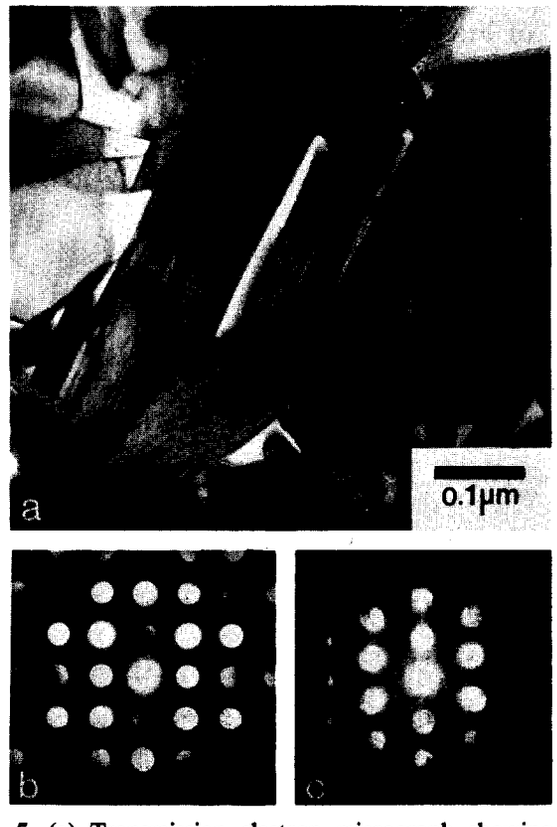

Fig. 5. (a) Transmission electron micrograph showing the morphology typical of elongated grains of the oxynitride-based phase (O), and electron microdiffraction patterns which can be indexed unambiguously as (b) [$1\bar{1}0$], and (c) [$\bar{1}01$] zone axis patterns from the orthorhombic oxynitride structure.

pockets was, however, rare, suggesting that the quantity of such phase within the microstructure was relatively small. Energy dispersive X-ray spectra, Fig. 7(a), recorded from the amorphous regions revealed significant concentrations of Si, Al, O, Ca and K; the C peak is a consequence of specimen coating and contamination. There was some evidence of the presence of nitrogen within the residual glass, but it proved difficult to detect because of the overlap of the adjacent oxygen and carbon peaks.

Microanalysis of the Si_2N_2O grains throughout the binder, Fig. 7(b), indicated the presence of significant concentrations of Al, along with Si, N, and O. It is thus suggested that the phase described thus far as an oxynitride is in fact an O-sialon ($Si_{2-x}Al_xO_{1+x}N_{2-x}$ with $x \leq 0{\cdot}2$). Similarly, significant concentrations of Al were also detected in the nitride grains in the binder, Fig. 7(c), suggesting that this phase is β-sialon ($Si_{6-z}Al_zO_zN_{8-z}$, $z < 4{\cdot}2$), formed by the limited substitution of Al^{3+} for Si^{4+}, with accompanying oxygen–nitrogen substitution for charge compensation.[23,24] The Si : Al ratio was observed to be constant, to within the limits of experimental error, in each of the two crystalline phases throughout the binder microstructure. This uniformity of composition would suggest that the liquid phase, which is the likely primary source of the Al and O, possesses a low viscosity, as would be expected for oxide liquid phases containing significant alkali-metal and alkaline earth concentrations,[25] and is uniformly distributed throughout the microstructure at the final reaction temperature of 1450°C.

Metallic inclusions were also observed occasionally at multiple grain junctions, and Fig. 8(a) shows an area containing a number of inclusions in dark contrast bounded by oxynitride grains. X-ray microanalysis, Fig. 8(b), indicated that the

Fig. 6. Representative transmission electron micrograph of microstructure of the composite matrix, showing discrete pockets of glassy phase (G) at three and four grain junctions.

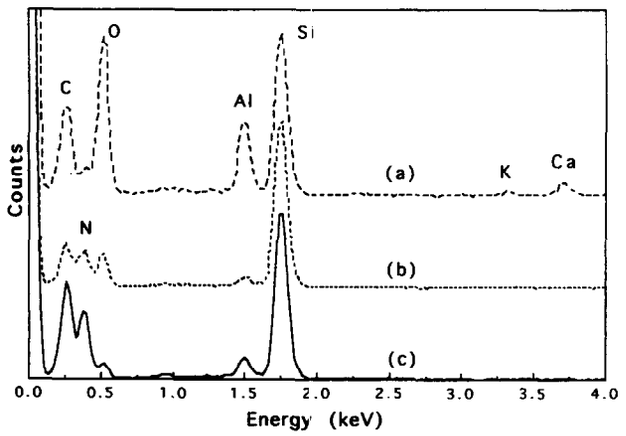

Fig. 7. Energy dispersive X-ray spectra typical of (a) amorphous phase, (b) O-sialon grains, and (c) β-sialon grains within the matrix of as-fired composite.

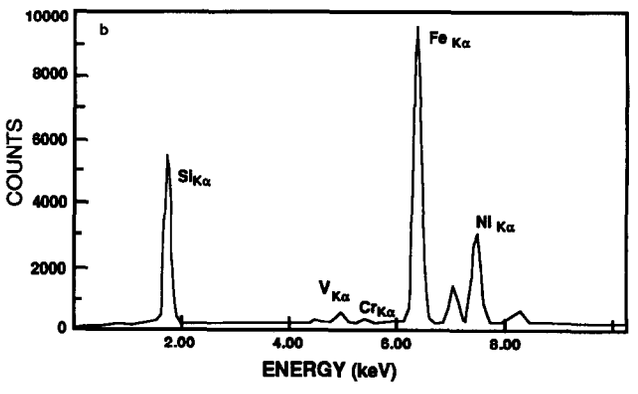

Fig. 8. (a) Transmission electron micrograph showing grains of metallic impurity phase within composite matrix, and (b) energy dispersive X-ray spectrum typical of the impurity phase.

particles contained significant concentrations of Fe, Si, Cr, Ni and V, and it seems likely that such inclusions are introduced during the attrition process, perhaps as a result of the use of stainless steel milling media.

Careful examination of a number of segments of the matrix/SiC interface typically indicated that the interface was cohesively bonded along the entire boundary length. No evidence of crack formation at the interface was observed and it also proved difficult to detect any amorphous thin films between the SiC and the binder phases. More detailed investigations of the interfacial region are in progress to elucidate the interface structure and to check for the presence of the amorphous intergranular films that are often reported in silicon nitride-based ceramics.[26–30]

An interesting feature of the microstructure was the common observation of the preferred nucleation of fine, rod-like O-sialon (O') grains along the boundaries of the coarse SiC particles. Figures 9(a) and (b) show a number of O' crystals extending outwards from their preferred nucleation sites on the SiC surface, with the preferred direction of elongation corresponding to the *c*-axis of the orthorhombic O' phase. Figure 10(a) is a composite electron microdiffraction pattern containing super-

Fig. 9. Transmission electron micrographs showing the preferred nucleation and growth of elongated O-sialon crystals from the surfaces of SiC grains.

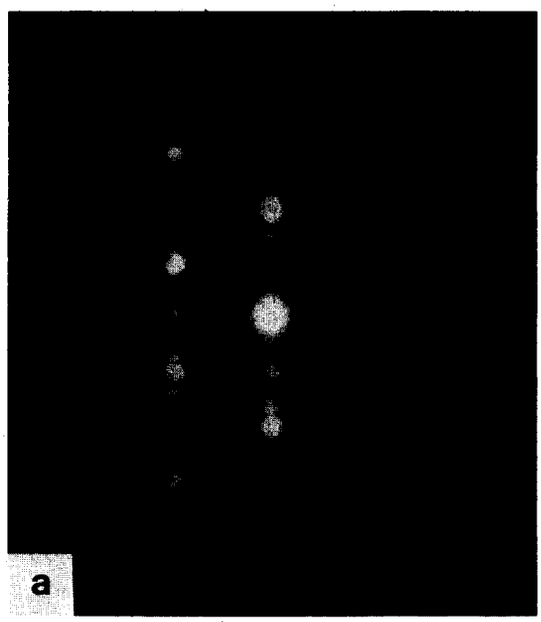

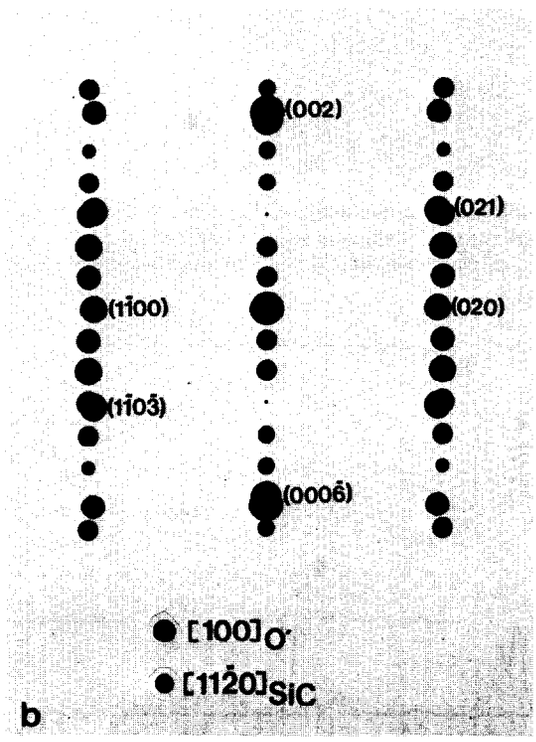

Fig. 10. (a) Composite electron microdiffraction pattern containing superimposed $[100]_{O'}$ and $[11\bar{2}0]_{SiC(6H)}$ zone axis patterns from adjoining regions of O-sialon and SiC, such as shown in Fig. 10, and (b) schematic solution to these patterns.

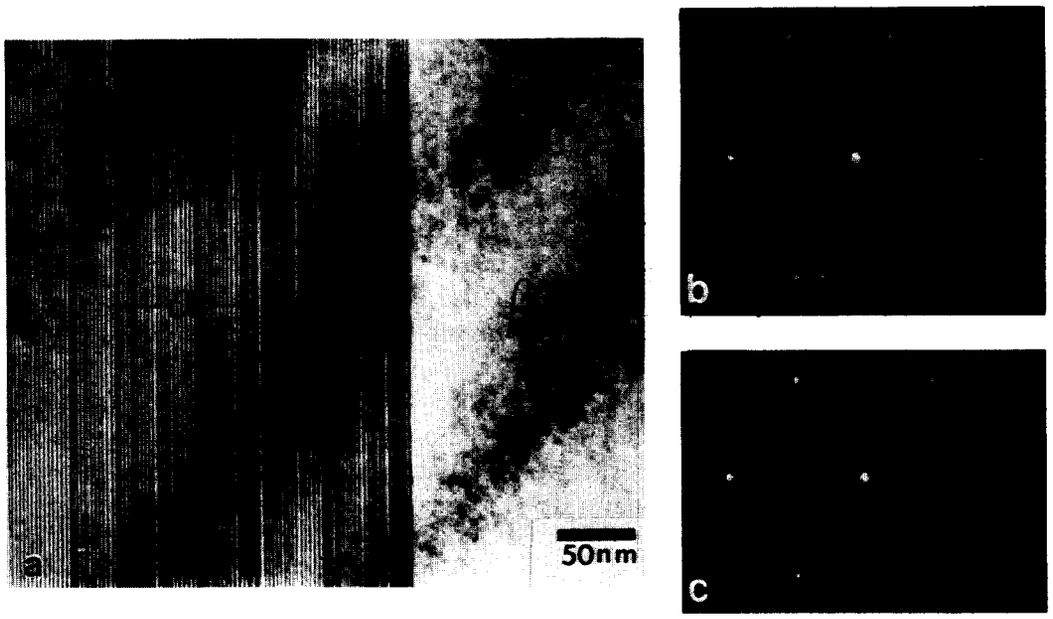

Fig. 11. (a) Transmission electron micrograph showing section of SiC grain containing regions of both the α- and β-SiC polymorphs, and corresponding (b) $[11\bar{2}0]_{SiC(6H)}$ and (c) $[110]_{SiC(\beta)}$ zone axis SAED patterns from the α and β structures respectively.

imposed zone axis patterns from adjoining regions of SiC and the O-sialon. As indicated by the schematic solution to the pattern in Fig. 10(b), the patterns imply an orientation relationship between the O' and the SiC in which:

$$(001)_{O'}// (0001)_{SiC}, \text{ and}$$

$$[100]_{O'}//[11\bar{2}0]_{SiC(6H)}.$$

Several regions in which β-sialon (β') grains were in direct contact with the SiC grains were also examined, but attempts to identify an orientation relationship[31] between the β' and the SiC have thus far been unsuccessful.

Examination of the large SiC particles using electron diffraction and lattice fringe imaging techniques[32] confirmed the existence of a variety of SiC polytypes, as suggested by the X-ray diffraction data from the composite (Fig. 1). The majority of areas examined with the electron beam parallel to a $<11\bar{2}0>$ direction exhibited lattice fringe spacings of 1·52 nm consistent with the 6H polymorph of α-SiC,[33] Fig. 11(a). However, a number of particles were observed to contain alternative α-SiC polytypes and, as illustrated in Fig. 11(a), local regions of β-SiC. The selected area electron diffraction pattern recorded from the α-SiC area in Fig. 11(a) and shown in Fig. 11(b) may be indexed for the hexagonal structure of the α-polytype. The streaking and additional low intensity reflections observed along the $\{10\bar{1}l\}$ diffraction row are characteristic of the faulted substructure of this polymorph.[33,34] In contrast, the SAED pattern in Fig. 11(c) may be indexed as the [110] zone axis pattern from β-SiC.

4 Discussion

Characterisation by analytical electron microscopy, in conjunction with X-ray diffraction, has established that the microstructure of the binder, in what is described as a Si_3N_4-bonded SiC composite, in fact comprises a mixture of crystalline phases based on Si_2N_2O and β-Si_3N_4, with a small volume fraction of residual amorphous phase rich in Si, Al, Ca, K and O. The high content of crystalline oxynitride and the almost exclusive appearance of β-Si_3N_4 (or β-sialon), both suggest the presence of a significant volume fraction of liquid phase during the 1450°C reaction bonding process, as those mechanisms proposed[12,14] for formation of Si_2N_2O invariably involve precipitation from a liquid phase, while the formation of β-sialon also commonly occurs from or in association with a liquid.[16] The residual glassy phase observed within the binder is consistent with the presence of a (Ca,K)–aluminosilicate derived liquid phase at the reaction temperature, although it is noted that the volume fraction of residual glassy phase is small in the as-fired product. These observations lead to a description of the consolidation of the composite in which the microstructure of the composite binder evolves via a modified solution–reprecipitation mechanism, such as that initially proposed for the reactive liquid–phase sintering of hot-pressed silicon nitride.[35,36]

In the case of the present Si/SiC powder composite preform, initial nitridation of the fine silicon powder during heating might be expected to lead to the formation of predominantly α-Si_3N_4 by

the vapour phase reaction of $Si_{(g)}$ or $SiO_{(g)}$ with nitrogen.[37] In the presence of Fe as a significant impurity, formation of the α phase might also arise[38] through Si vaporisation from any $FeSi_x$ liquid phase that may form. However, in studies of the reaction bonding of Si_3N_4 there are numerous reports of the formation of a product containing a significant volume fraction of β-Si_3N_4 at temperatures as low as 1330°C,[38] and it has been suggested[38] that the development of the two modifications may be determined by particular growth mechanisms. The choice of growth mechanism may be strongly influenced by the presence or otherwise of significant fractions of low melting point liquid phase generated from the natural oxide film on the original powder(s) and/or other impurity ingredients.

It is also well established that α-Si_3N_4 transforms to β-Si_3N_4 during heat treatment at temperatures in the vicinity of 1500°C,[17] and that this transformation may be facilitated by the presence of impurity elements and/or a liquid phase of appropriate composition.[16] There are thus at least two mechanisms by which the β-Si_3N_4 observed in the as-fired product may form and increase in volume fraction during the reaction cycle. It is noteworthy that two distinguishable morphologies of the β-nitride were observed within the binder; the major fraction contained rounded, equiaxed grain shapes, but there was a small fraction of grains possessing a faceted and elongated form more typical of a product forming as a precipitate from a liquid phase. These different grain shapes may constitute evidence of two different growth mechanisms contributing to the total fraction of β-Si_3N_4 in the binder.

The EDXS analyses of residual amorphous regions in the composite imply the existence at the reaction temperature of a (Ca,K)–aluminosilicate based liquid phase with a composition derived principally from the clay addition. The timing of the formation of this liquid phase in the reaction sequence may have a strong influence on phase formation within the microstructure. The formation of an extensive liquid phase early in the reaction sequence may, for example, inhibit the formation of Si_3N_4[3] by the premature closure of the pore network necessary for the access of nitrogen to the silicon, if indeed direct access of nitrogen to solid silicon is essential to continuing nitridation. This might be expected to lead to a large residual silicon content in the sintered product. However, both X-ray diffraction and direct microscopic observation indicate that only a small fraction of silicon remains within the present composite. Given that the melting point of the liquid phase is likely to be low (<1450°C) and the liquid phase is thus likely to be present from the earliest stages of the reaction bonding sequence, this suggests that the volume fraction and viscosity of the liquid phase, combined with the low green density of the compact, are such that they do not adversely affect the access of the nitrogen to the silicon.

In the initial stages of nitridation it seems likely that the product is a mix of α-Si_3N_4 formed via a gas phase reaction and β-Si_3N_4 formed perhaps by a combination of mechanisms involving the presence of the (Ca,K)–aluminosilicate liquid phase. Exposed to an increasing fraction of oxygen-rich liquid phase at the reaction temperature, the less stable α-Si_3N_4 present will dissolve to form essentially calcium sialon liquid, and be replaced by the precipitation of the Si_2N_2O-based phase. The large volume fraction of O' compared with β' in the binder is consistent with a substantial proportion of the (α-)Si_3N_4 formed by nitridation being consumed by the liquid phase, while the elongated, faceted morphology and faulted substructure of grains of this phase are characteristic of the oxynitride forming from a liquid phase.[20] It is to be expected that the relatively low solubility of nitrogen combined with a high oxygen activity in the liquid phase will favour formation of O-sialon.

The direct observation of aluminium within the Si_2N_2O-based phase, together with the measurement of lattice parameters systematically larger than the range of lattice constants reported for pure Si_2N_2O, confirm the identity of the phase as O'. The lattice parameter a of O' experiences the most significant expansion as the result of the replacement of Si^{4+} ions with Al^{3+} ions, and comparison of the present measured values with published results[39,40] suggests that the aluminium content of the O-sialon ($Si_{2-x}Al_xO_{x+1}N_{2-x}$) is such that $x \geq 0{\cdot}14$ and, according to some observations,[40] approaching the limit of aluminium solubility in the O' structure. This is consistent with the precipitation of the O' from a liquid phase in which the activity of aluminium is high, i.e. a liquid phase forming in the presence of a high Al_2O_3 concentration.

A unique feature of the present study was the common observation of elongated grains of the oxynitride-based phase extending from the surface of coarse SiC particles and sustaining a well-defined orientation relationship with the SiC. This orientation relationship is such that the long axis of the O', $[001]_{O'}$, is parallel to the c axis of the 6H SiC, and the misfit between $(002)_{O'}$ and $(0006)_{SiC(6H)}$ planes normal to the preferred growth axis is approximately 3·3%, based on lattice parameters determined at room temperature. Normal to the interface between the O' and the SiC, Fig. 10(a),

the planes $(020)_{O'}$ and $(1\bar{1}00)_{SiC}$ are approximately parallel and contain the growth axis, and differ in spacing by only approximately 2·9%. Similarly, the planes $(100)_{O'}$ and $(11\bar{2}0)_{SiC}$ are parallel across the interface and the misfit between them is approximately 3·3%. The form of these O' grains, and the relatively low lattice misfit between the O' and the SiC phases in the observed orientation relationship, imply the preferred heterogeneous nucleation of the Si_2N_2O-based grains on the SiC and their subsequent growth outward into surrounding liquid phase. That they grow into liquid phase is supported by the common observation of small glass pockets surrounding these grains in the as-fired product.

Regardless of the mechanism of formation of the β' phase, the direct observation of aluminium (and oxygen) within the various grain morphologies, together with the magnitudes of the measured lattice parameters, confirm the identification of this phase as β-sialon rather than β-Si_3N_4. There were no significant variations detectable in the aluminium concentration within the different β-sialon morphologies and across many grains of each analysed using EDXS. This suggests that the extended hold time at the final sintering temperature of 1450°C may be sufficient to allow the aluminium and oxygen concentrations within both the β' and O' to approach saturation in the solid state at this temperature. In the case of any β' formed as a solid state reaction product this would seem to imply the diffusion of aluminium and oxygen from the aluminium-rich liquid phase during or immediately following initial nitridation.

If measured values of the lattice parameters for the crystalline binder phases are compared with existing data[41,42] to determine the values of z and x for the β' ($Si_{6-z}Al_zO_zN_{8-z}$) and O' phases respectively, the results support the notion that the aluminium concentration approaches saturation within both phases during the firing treatment. The calculated values of $z = 0{\cdot}45$ and $x = 0{\cdot}14$ are equivalent to aluminium concentrations of 5·72 and 5·34 eq% respectively, indicating that, to within reasonable error limits, the aluminium content of the two phases is essentially identical.

The presence of residual glass pockets in the final microstructure results from a failure to completely exhaust the supply of liquid phase at the reaction temperature. It is noteworthy that the pockets of glass, such as shown in Fig. 4, were relatively rare and that the volume fraction of residual glass was relatively small. There would thus seem to exist, potential for largely eliminating residual glassy phase from the final microstructure through improved design of the composition of the composite and, in particular, improved control of the additions of those minor constituents which generate and stabilise the liquid phase during processing.

5 Summary

(1) The microstructure of the commercial silicon nitride-bonded silicon carbide ceramic composite, formed via the nitridation of silicon powder–SiC preforms, comprises coarse particles of SiC dispersed in a matrix or binder which is a mixture of crystalline phases based on Si_2N_2O and β-Si_3N_4 in the volume ratio of approximately 2:1, together with a small volume fraction of residual amorphous phase.

(2) The direct observation of significant concentrations of aluminium (and oxygen) within both of the crystalline phases, together with measured lattice parameters which are systematically larger than those of the pure compounds, imply that the crystalline phases within the binder are in fact O- and β-sialons respectively.

(3) The O-sialon is observed to nucleate preferentially, but not exclusively, on the 6H SiC particles with an orientation relationship with the SiC of the form:

$$(001)_{O'}// (0001)_{SiC}, \text{ and}$$
$$[100]_{O'}//[11\bar{2}0]_{SiC(6H)}.$$

(4) Direct qualitative microanalysis of amorphous matrix regions indicates the presence of significant concentrations of aluminium, silicon, calcium and oxygen. The regions are interpreted to represent the residue of a reactive, low melting point (Ca,K)–aluminosilicate liquid phase, deriving predominantly from clay binder additions to the original powder mix and present throughout the reaction sequence.

(5) It is proposed that the β-sialon within the binder is predominantly the product of a reaction-bonding sequence, perhaps facilitated by the presence of the liquid phase. The O' is suggested to arise as a result of the dissolution of α-Si_3N_4 in the oxygen-rich liquid phase, followed by precipitation of the O-sialon.

Acknowledgement

One of the authors (D.P.E.) gratefully acknowledges the award of a Postgraduate Research Fellowship under the auspices of the Australian Government Cadet Research Scientist Scheme.

References

1. Falk, L. K. L., Pompe, R. & Dunlop, G. L., Development of microstructure during nitridation and sintering of Si:Si_3N_4 Powder Compacts. In *Science of Ceramics 12*, ed. P. Vincenzini, Ceramurgica S. R. L., Faenza, Italy, 1984, p. 293.
2. Pompe, R., Hermansson, L. & Carlsson, R., Fabrication of low-shrinkage silicon nitride material by pressureless sintering, In *Engineering with Ceramics*, British Ceramics Society, Stoke-on-Trent, ed. R. W. Davidge, 1982, p. 65.
3. Brown, I. W. M., Pompe, R. & Carlsson, R., Preparation of sialons by the nitrided pressureless sintering (NPS) technique. *J. Eur. Ceram. Soc.*, **6** (1990) 191.
4. Falk, L. K. L., Dunlop, G. L. & Pompe, R., The microstructure of Si_3N_4 formed by nitridation and pressureless sintering of Si–Si_3N_4 compacts. *Mater. Sci. Eng.*, **71** (1985) 123.
5. Morrison, F. C. R., Maher, P. P. & Hendry, A., In-situ formation of sialons in refractories containing silicon carbide. *Brit. Ceram. Trans. J.*, **88**(5) (1989) 157.
6. Arrol, A. J., Ceramics for high performance applications. *Proc. 2nd Army Materials Technology Conference*, Hyannis, Massachusetts 1973, p. 729.
7. Zhiping, Z., Hui-Hang, H. & Zhao Hui, H., Sialon-bonded SiC refractories for blast furnace. *Interceram*, **42**(5) (1993) 292.
8. Scott, H., Celsiz program, C.S.I.R.O. Division of Materials Science and Technology, Victoria, Australia.
9. Liddell, K., X-ray analysis of nitrogen ceramic phases, M.Sc. Thesis, University of Newcastle upon Tyne, UK, (1979).
10. Schneider, M., Edv-Vetrieb, WYRIET, Version 3, Starnbergerweg 18, D-8134 Pöcking, Germany.
11. Powder Diffraction File, JCPDS-ICDD, 1990.
12. Trigg, M. B. & Jack, K. H., Silicon oxynitride and O'SiAlON ceramics. *Proc. of International Symposium on Ceramics Components for Engines*, ed. S. Somiya, E. Kanai & K. Ando, Tokyo, Japan, 1983, p. 199.
13. Bergman, B. & Heping, H., The influence of different oxides on the formation of Si_2N_2O from SiO_2 and Si_3N_4. *J. Eur. Ceram. Soc.*, **6** (1990) 3.
14. Huang, Z. K., Greil, P. & Petzow, G., Formation of silicon oxynitride from Si_3N_4 and SiO_2 in the Presence of Al_2O_3. *Ceram. Int.*, **10**(1) (1984) 14.
15. Ness, J. N. & Page, T. F., The structure and properties of interfaces in reaction-bonded silicon carbides. In *Tailoring Multiphase and Composite Ceramics*, Materials Science Research, Vol. 20, ed. R. E. Tressler, G. L. Messing, C. G. Pantano & R. E. Newnham, Penn., USA, 1985, p. 347.
16. Braue, W., Wotting, G. & Ziegler, G., The impact of compositional variations and processing conditions on secondary phase characteristics in sintered silicon nitride materials. In *Ceramic Microstructures '86, Role of Interfaces*, eds J. A. Pask & A. G. Evans. *Mater. Sci. Res.*, **21** 1987, p. 883.
17. Messier, D. R., Riley, F. L. & Brook, R. J., The α/β silicon nitride phase transformation. *J. Mater. Sci.*, **13** (1978), 1199.
18. Ziegler, G., Heinrich, J. & Wotting, G., Review: relationships between processing, microstructure and properties of dense reaction-bonded Silicon Nitride. *J. Mater. Sci.*, **22** (1987) 3041.
19. Siddiqi, S. A. & Hendry, A., The microstructure of dense, low cost silicon oxynitride. *Special Ceramics 8*, (1985) 1.
20. Lewis, M. H., Reed, C. J. & Butler, N. D., Pressureless-sintered ceramics based on the compound Si_2N_2O. *Mater. Sci. Eng.*, **71** (1985) 87.
21. Sjoberg, J., Helgesson, G. & Idrestedt, I., Refinement of the structure of Si_2N_2O. *Acta Cryst*, **C47** (1991) 2438–41.
22. Clarke, D. R., Application of electron microscopy to the processing of ceramic materials. *Ultramicroscopy*, **8** (1982) 95.
23. Jack, K. H., Review: sialons and related nitrogen ceramics. *J. Mater. Sci.*, **11** (1976), 1135.
24. Trigg, M. B. & Jack, K. H., The fabrication of O'-sialon ceramics by pressureless sintering. *J. Mater. Sci.*, **23** (1988) 481.
25. Jastrzebski, Z. D., *The Nature and Properties of Engineering Materials, 2nd Edition*, J. Wiley & Sons Inc., 1977.
26. Das Chowdhury, K., Carpenter, R. W. & Braue, W., A comparative high-resolution study of interface chemistry in silicon-nitride-based ceramic matrix composites reinforced with silicon carbide whiskers. *Ultramicroscopy*, **40** (1992) 229.
27. More, K. L, Koester, D. A. & Davis R. F., Microstructural characterization of a creep-deformed SiC whisker-reinforced Si_3N_4. *Ultramicroscopy*, **37** (1991) 263.
28. Clarke, D. R., Zaluzec, N. J. & Carpenter, R. W., The intergranular phase in hot-pressed silicon nitride: 1. Elemental Composition. *J. Am. Ceram. Soc.*, **64**(10) (1981) 601.
29. Lou, L. K. V., Mitchell, T. E. & Heuer, A. H., Discussion of grain boundary phases in a hot-pressed MgO fluxed silicon nitride. *J. Am. Ceram. Soc.*, **61**(9–10) (1978) 462.
30. Kleebe, H. J., Cinibulk, M. K., Cannon, R. M. & Ruhle, M., Statistical analysis of the intergranular film thickness in silicon nitride ceramics. *J. Am. Ceram. Soc.*, **76**(8) (1993) 1969.
31. Unal, O., Petrovic, J. J. & Mitchell, T. E., CVD Si_3N_4 on Single Crystal SiC: Part 1. Characterization and orientation relationship at the interface. *J. Mater. Res.*, **7**(1) (1992) 136.
32. Clarke, D. R., High-resolution techniques and applications to non-oxide ceramics. *J. Am. Ceram. Soc.*, **5–6** (1979) 236.
33. Dubey, M., Singh, G. & Van Tendeloo, G., X-ray and transmission electron microscopy study of extremely large-period polytypes in SiC. *Acta. Cryst.*, **A33** (1977) 276.
34. Ogbuji, L. U., Mitchell, T. E. & Heuer, A. H., The β–α transformation in polycrystalline SiC: III. The thickening of α plates. *J. Am. Ceram. Soc.*, **64**(2) (1981) 91.
35. Lewis, M. H., Powell, B. D., Drew P., Lumby, R. J., North, B. & Taylor, A. J., The formation of single-phase Si–Al–O–N ceramics. *J. Mater. Sci.*, **12** (1977), 61.
36. Hampshire, S. & Jack, K. H., The kinetics of densification and phase transformation of nitrogen ceramics. *Proc. Brit. Ceram. Soc.*, **31** (1981) 37.
37. Blegen, K., Equilibria and kinetics in the systems Si–N and Si–N–O. *Special Ceramics 6*, Proc. 6th Symp. on Special Ceramics, B.C.R.A., 1974, p. 223.
38. Moulson, A. J., Review: Reaction-bonded silicon nitride: its formation and properties. *J. Mater. Sci.*, **14** (1979) 1017.
39. Trigg, M. B. & Jack, K. H., Solubility of aluminium in silicon oxynitride. *J. Mater. Sci. Let.*, **6** (1987) 407.
40. Lindqvist, O., Sjoberg, J., Hull, S. & Pompe, R., Structural changes in O'-sialons, $Si_{2-x}Al_xO_{1+x}N_{2-x}$, $0{\cdot}04<x<0{\cdot}4$, *Acta Cryst.*, **B47** (1991) 672.
41. Haviar, M. & Johannesen, F., Unit-cell dimensions of β'-sialons, *Adv. Ceram. Mater.*, **4** (1988) 405.
42. Ohashi, M., Hirao, K., Brito, M. E., Takaaki, N., Yasuoka, M. & Kanzaki, S., Solid solubility of aluminium in O'-SiAlON. *J. Am. Ceram. Soc.*, **76**(8) (1993) 2112.